ChemComm

COMMUNICATION

View Article Online
View Journal

Cite this: DOI: 10.1039/d5cc06634d

Received 21st November 2025,
Accepted 18th December 2025

DOI: 10.1039/d5cc06634d

rsc.li/chemcomm

Insights into the crystal packing interactions of a 960-nm-emissive DNA-stabilized silver nanocluster

Giacomo Romolini, †[a] Hiroki Kanazawa, †[b] Simon Wentzel Lind, [a] Cecilia Cerretani, [a] Christian Brinch Mollerup, [c] Letizia Liccardo, [a] Zhiyu Huang, [a] Leila Lo Leggio, [a] Vanessa Rück, [a] Jiro Kondo *[b] and Tom Vosch *[a]

DNA-stabilized silver nanoclusters (DNA-AgNCs) can be finely tuned through DNA sequence design. Here, we present mutations in a DNA strand that stabilize an $[Ag_{28}Cl_2]^{14+}$ cluster, which remains largely unaltered, as confirmed by spectroscopy and mass spectrometry. The crystal structure of one mutant further reveals previously unseen packing interactions among DNA-AgNCs.

DNA-stabilized silver nanoclusters (DNA-AgNCs) have emerged as a unique class of emissive materials due to remarkable photophysical properties such as tunable emission, high fluorescence quantum yields, and a large range of excited state decay times (ps to μs-range).[1–10] DNA-AgNCs are formed through the coordination of silver to nucleobases, where the DNA acts both as a structural scaffold and as a chemical modulator of the nanocluster's size, geometry, and optical features.[11–16] Despite rapid progress in the development of DNA-AgNCs, our knowledge of the sequence-structure relationship remains incomplete. Understanding how individual nucleotide modifications control DNA-AgNC formation and affect photophysical properties is crucial for establishing a rationale and developing predictive tools.[17–19] In this study, we explore the role of positions 3 and 8 in the DNA sequence (5′-CCGCGCGCGCCGCGAA-3′) that was recently reported to stabilize a 960 nm-emitting DNA_2-$[Ag_{28}Cl_2]^{14+}$ cluster (further referred to as C8).[18] Single crystal X-ray data revealed that the cytosine in position 8, C_8 (subscripts on the DNA nucleobases are used to specify the position of each individual base), pointed away from the AgNC and was only responsible for crystal packing interactions with a guanine (G_3) of a neighboring DNA-AgNC unit.[18] As such, this information led us to hypothesize that position 8 could be modified with other nucleobases (A8, G8, T8) or even removed from the sequence (–C8). The G_3 coordinates the AgNC through its N7 atom, allowing for Watson–Crick pairing with a close C_8 base. Guided by this unique interaction feature, we replaced G_3 with A_3 to generate the A3 and A3T8 mutants. Like guanine, adenine features an N7 site capable of coordinating the AgNC, and we sought to evaluate whether a Watson–Crick–type interaction could form between the A_3 and the T_8 of two adjacent clusters in the A3T8 crystals. We were able to grow crystals for most of the modifications, and we solved the structure of the T8 variant, providing new information on crystal packing interactions between DNA-AgNCs. We demonstrated that the solution properties of all the selected mutants (A8, G8, T8, –C8, A3T8, and A3) are very similar to the original C8 version.

The synthetic protocol for all variants, along with details of the HPLC purification, is provided in the SI. Briefly, we performed a synthesis screening by monitoring the absorbance peak at 835 nm, indicative of the presence of the DNA_2-$[Ag_{28}Cl_2]^{14+}$ cluster in the reaction batch. For most mutations, the highest absorbance peak at 835 nm was observed at 72 hours (see Fig. S1). Therefore, for consistency, purification of all the mutants was carried out 3 days after starting the reaction. Fig. S2–S7 show the HPLC chromatograms of the new variants presented in this paper. The spectroscopic properties of the purified mutants were remarkably similar to those already reported for C8.[18] The absorption maxima were similar and situated around 835 nm, while the emission maxima were around 960 nm for the position 8 modifications (See Fig. 1). Interestingly a minor blue-shift of about 19 nm and 10 nm in the emission spectra was observed for A3 and A3T8, respectively. It is also worth noting that the synthesis yield and quality of the HPLC purification varied from mutant to mutant and led to the observed discrepancies in the 300–700 nm range, indicating the presence of some by-products. However, as shown below, the minor impurities did not affect the photophysical properties of the variants or their ability to form crystals. Furthermore, the fluorescence quantum yields were found to be very similar to that of C8 (see Table 1 and Fig. S14). In line

[a] Department of Chemistry, University of Copenhagen, Universitetsparken 5, DK-2100, Copenhagen, Denmark. E-mail: tom@chem.ku.dk
[b] Department of Materials and Life Sciences, Sophia University, 7-1 Kioi-cho, Chiyoda-ku, 102-8554, Tokyo, Japan. E-mail: j.kondo@sophia.ac.jp
[c] Department of Forensic Medicine, University of Copenhagen, Frederik V's Vej 11, DK-2100, Copenhagen, Denmark
† Contributed equally.

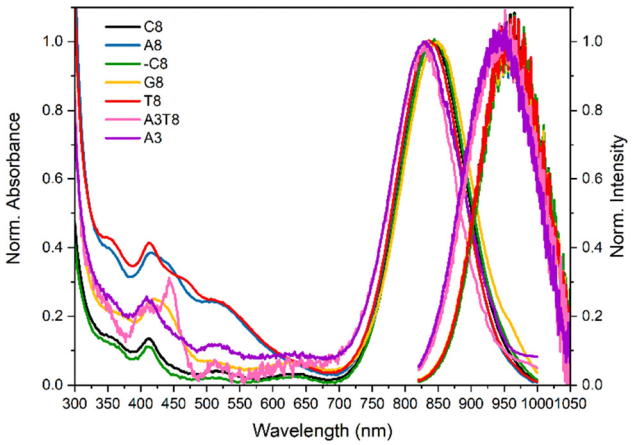

Fig. 1 Normalized absorption and emission spectra of the original DNA_2-$[Ag_{28}Cl_2]^{14+}$ (C8, black), and the mutations introduced in this study: A8 (blue), −C8 (green), G8 (yellow), T8 (red), A3T8 (pink), and A3 (purple). The emission spectra were recorded by exciting at 790 nm.

with this, the fluorescence decay times were also alike, spanning from 0.72 to 0.79 ns (see Table 1 and Fig. S8–S13). As hypothesized, mutating position 8 or removing the cytosine in this position did not alter the intrinsic spectroscopic properties of the DNA_2-$[Ag_{28}Cl_2]^{14+}$ cluster (C8) in solution, while changing position 3 from guanine to adenine only led to minimal changes.

Electrospray ionization-mass spectrometry (ESI-MS) was employed to verify that the AgNCs in all mutants were compositionally consistent with the original C8.[18] We previously reported a discrepancy between the chemical composition observed in the crystal structure (DNA_2-$[Ag_{28}Cl_2]^{14+}$) and in solution (DNA_2-$[Ag_{28}]^{16+}$).[18] This difference made us speculate that the chlorido ligands may not bind strongly in this particular DNA-AgNC, and therefore might not be readily detected in mass spectrometry experiments. However, the addition of about a hundredfold excess of NaCl led to the decrease of the DNA_2-$[Ag_{28}]^{16+}$ molecular ion peak and the rise of the DNA_2-$[Ag_{28}Cl]^{15+}$ peak (although no clear DNA_2-$[Ag_{28}Cl_2]^{14+}$ was detected).[18] ESI-MS analyses of the A8, T8, G8, −C8, A3T8, and A3 mutants revealed that all the mutations consistently yielded DNA_2-$[Ag_{28}]^{16+}$ cluster as the main species (see Fig. 2 and Fig. S15–S22). Interestingly, even though the same ionization

Table 1 Fluorescence quantum yields and intensity averaged decay times (τ) of the C8, A8, T8, G8, −C8, A3T8, A3 DNA-AgNCs

Mutant	Quantum yield	τ (ns)
C8[a]	0.12	0.74
A8	0.11	0.72
T8	0.11	0.74
G8	0.11	0.74
−C8	0.11	0.72
A3T8	0.12	0.76
A3	0.13	0.79

Fluorescence decays are shown in Fig. S8–S13, while absorption and emission spectra used for quantum yield determination are reported in Fig. S14. Excitation wavelength was 790 nm. [a] The C8 data are from ref. 18.

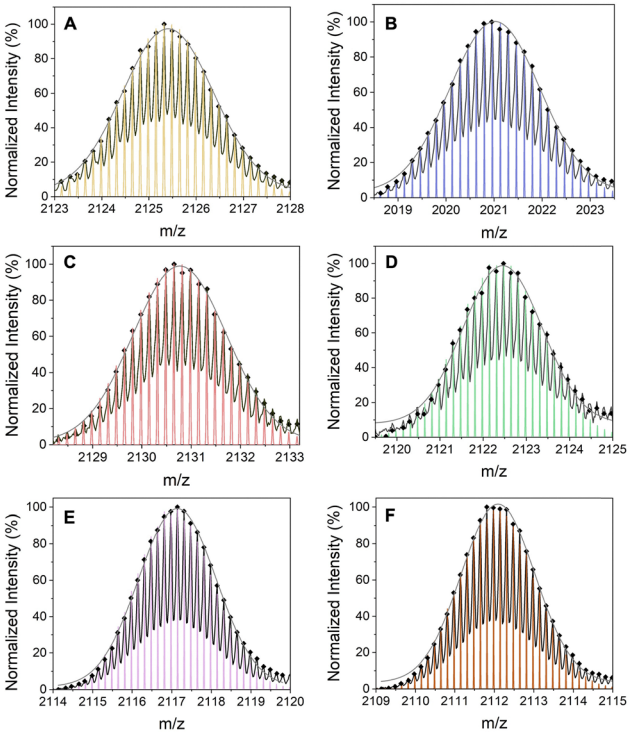

Fig. 2 Mass spectrometry data showing the molecular ion peak corresponding to DNA_2-$[Ag_{28}]^{16+}$ with a 6^- charge state for (A) A8, (B) −C8, (C) G8, (D) T8, (E) A3T8, and (F) A3. The experimental peaks are reported along with the theoretical isotopic distributions and Gaussian fits. The calculated average masses (μ) are reported in Fig. S16A, S17A, S18A, S19A, S20A and S21A, respectively.

conditions were applied as in the previous experiments, the mass spectra now prominently feature peaks associated with single chlorido adducts, DNA_2-$[Ag_{28}Cl]^{15+}$ (Table S2), except for A3T8 and A3. Moreover, similarly to the C8 compound, mass spectrometry data of all variants show no clear peaks associated with DNA_2-$[Ag_{28}Cl_2]^{14+}$ adducts.[18] While one could hypothesize that the differences observed in the mass spectra could be associated with different binding affinities of the mutants for chloride ions, we cannot exclude that they merely reflect differences in the chloride impurity levels throughout the synthesis, storage and measurement process.

Once the photophysical properties and molecular formula of the mutations were confirmed, we screened several crystallization conditions. All the mutants, except A3, easily crystallized within a week, producing dark green crystals (see Fig. S16 for selected examples). Further details on the crystallization can be found in the SI. All crystals displayed fluorescence maxima in the 950–1050 nm range (Fig. S15), consistent with the red shift previously reported for C8 in the crystalline state.[18] Although crystals were successfully grown for most variants, high-quality diffraction data were obtained only for the T8 mutant, allowing structure determination.

The structure and experimental data have been deposited in the Protein Data Bank (PDB) with the accession code 9XRW. The crystal structure of the T8 mutant reveals significant differences in packing compared to the original C8 (PBD

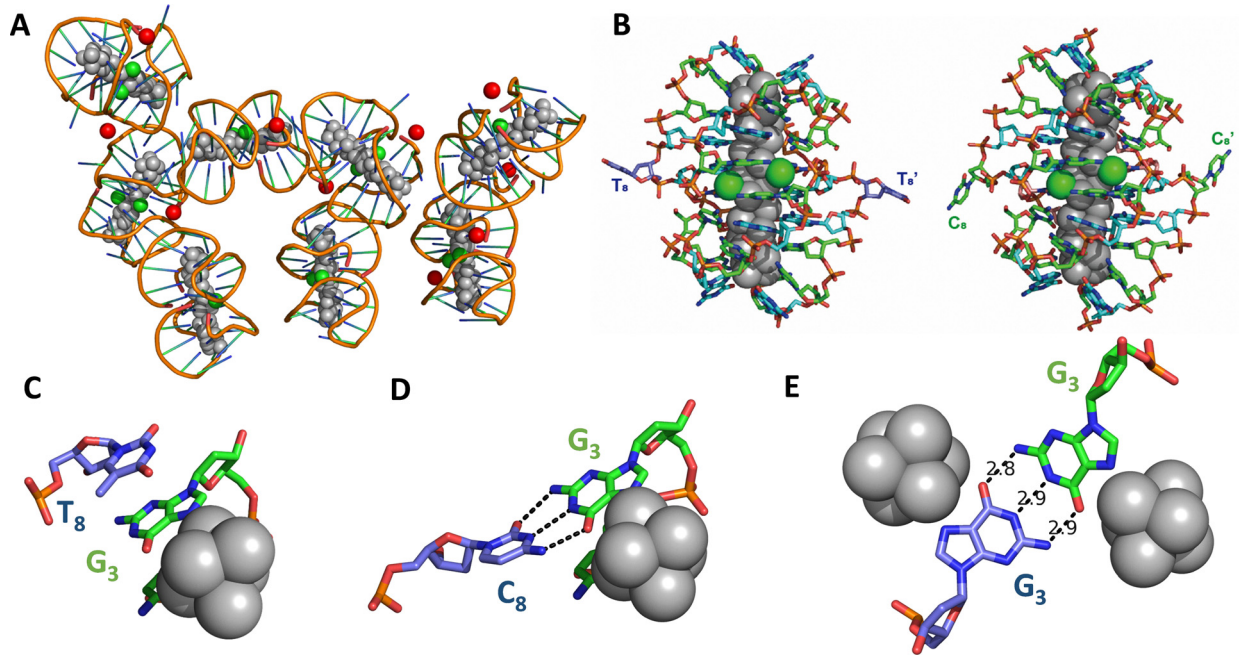

Fig. 3 (A) Asymetric unit of the T8 mutant containing eight DNA_2-$[Ag_{28}Cl_2]^{14+}$ clusters. Silver, chlorine and strontium atoms are represented as gray, green and red spheres, respectively. (B) Comparison of a single DNA_2-$[Ag_{28}Cl_2]^{14+}$ cluster of the T8 mutant and the original C8. (C) π-stacking interaction between T_8 and G_3 from neighboring DNA_2-$[Ag_{28}Cl_2]^{14+}$ clusters in the T8 variant crystal. (D) Watson–Crick base pair between C_8 and G_3 from adjacent DNA_2-$[Ag_{28}Cl_2]^{14+}$ clusters in the C8 mutant crystal. (E) *Trans* Watson–Crick base pair interaction between G_3s belonging to neighboring DNA_2-$[Ag_{28}Cl_2]^{14+}$ clusters in the T8 crystal. Bond lengths are given in Å.

9KHW), despite both crystallizing in the $P2_1$ space group. The unit cell of T8 (a = 33.6 Å, b = 108.1 Å, c = 108.2 Å, β = 90.03°) is notably larger than C8 (a = 27.2 Å, b = 53.2 Å, c = 27.2 Å, β = 103.67°), indicating a substantial reorganization of the crystal packing. In fact, the asymmetric unit of the T8 crystal contains eight DNA_2-$[Ag_{28}Cl_2]^{14+}$ molecules (Fig. 3A) compared to only one in the original C8. Despite the increased number of DNA_2-$[Ag_{28}Cl_2]^{14+}$ clusters in the unit cell, the overall architecture of the metal core remains highly conserved, with a maximum RMSD of 0.16 Å for the silver cluster atoms and 0.4 Å when the DNA strands are also included in the calculations (see Fig. S24 and S25). The minor deviations observed among subunits primarily arise from slight variations in the orientation of the DNA backbones and local packing effects, rather than any significant rearrangement of the AgNC framework. Given the similarities of the T8 and C8 overall structures (Fig. 3B), we refer to our previous work for a detailed description of the DNA_2-$[Ag_{28}Cl_2]^{14+}$ structure itself.[18] For the T8 mutation, we were able to locate strontium ions from the crystallization buffer (see red spheres in Fig. 3A). These ions, coordinated by water molecules with a Sr–O distance of 2.7 ± 0.2 Å, additionally enhance the crystal packing. Fig. 3B shows that for some of the DNA_2-$[Ag_{28}Cl_2]^{14+}$ units, the T_8 nucleotide points towards a neighboring DNA_2-$[Ag_{28}Cl_2]^{14+}$ cluster and forms π-stacking interactions with the G_3 base (Fig. 3C). This interaction replaces the Watson–Crick base pair between C_8 and G_3 that is present in the original C8 structure (Fig. 3D). Another intriguing interaction arises from the three hydrogen bonds formed between two G_3 nucleotides in adjacent DNA_2-$[Ag_{28}Cl_2]^{14+}$ clusters (see Fig. 3E). The bond length of 2.9 Å between the two N1 atoms of the guanines suggests that one of them is deprotonated.

In conclusion, we investigated the effects of nucleotide substitutions at positions 3 and 8, as well as the deletion of position 8, in the DNA sequences that stabilize the $[Ag_{28}Cl_2]^{14+}$ cluster. Our findings reveal that the nucleobase at position 8 is not essential for the formation or photophysical properties of the 960 nm emitter, but it has an impact on the synthesis yield. Mass spectrometry analysis revealed consistent formation of DNA_2-$[Ag_{28}]^{16+}$ clusters across all mutations. At position 3, the original guanine was replaced with adenine. Both the A3T8 and A3 mutants displayed similar spectroscopic properties. Crystals were obtained for all variants except A3, and we successfully determined the structure of the T8 mutant. The structure of T8 showed significant differences in the crystal packing arrangement compared to that of the original C8, including a larger asymmetric unit with eight DNA_2-$[Ag_{28}Cl_2]^{14+}$ clusters. The crystal packing interactions include T_8-G_3 π-stacking and non-canonical G_3–G_3 base pairs between adjacent DNA_2-$[Ag_{28}Cl_2]^{14+}$ clusters. As such, these targeted mutations provide a foundation for future design strategies and enable validation of predicted structural and photophysical outcomes.

Conflicts of interest

There are no conflicts to declare.

Data availability

The data supporting this article have been included as part of the supplementary information (SI) of this article and at https://doi.org/10.5281/zenodo.17591636. Crystallographic data for the T8 mutant has been deposited at PDB under accession code 9XRW. Supplementary information is available. See DOI: https://doi.org/10.1039/d5cc06634d.

Acknowledgements

G. R., S. W. L., V. R., C. C. and T. V. acknowledge funding from the Villum Foundation (VKR023115), the Independent Research Fund Denmark (0136-00024B) and the Novo Nordisk Foundation (NNF22OC0073734). G. R. acknowledges funding by the European Union (MSCA, NIR-emitting Ag-DNAs 101151897). Views and opinions expressed are those of the author(s) only and do not necessarily reflect those of the European Union or the Research Executive Agency. Neither the European Union nor the granting authority can be held responsible for them. We acknowledge MAX IV Laboratory for time on Beamline Biomax under Proposal 20240265 allocated to L. L. L. Research conducted at MAX IV, a Swedish national user facility, is supported by the Swedish Research council under contract 2018-07152, the Swedish Governmental Agency for Innovation Systems under contract 2018-04969, and Formas under contract 2019-02496. We thank the Danish Agency for Science, Technology, and Innovation for funding the instrument center DanScatt, supporting travel and sample shipping to synchrotrons and MAX IV staff for assistance during the beamtime. Z. H. was funded by the Independent Research Fund Denmark (Natural Sciences) under grant 3103-00279B to L. L. L. J. K. and H. K. thank the Research Support Project for Life Science and Drug Discovery (Basis for Supporting Innovative Drug Discovery and Life Science Research (BINDS)) from AMED under Grant Number JP23ama121014.

References

1 A. Gonzàlez-Rosell, C. Cerretani, P. Mastracco, T. Vosch and S. M. Copp, *Nanoscale Adv.*, 2021, **3**, 1230–1260.
2 J. T. Petty, S. Carnahan, D. Kim and D. Lewis, *J. Chem. Phys.*, 2021, **154**, 244302.
3 A. Gonzàlez-Rosell, R. Guha, C. Cerretani, V. Rück, M. B. Liisberg, B. B. Katz, T. Vosch and S. M. Copp, *J. Phys. Chem. Lett.*, 2022, **13**, 8305–8311.
4 K. Woloszyn, L. Perren, J. Janowski, L. Faiaz, V. R. Singh, M. Jaffe, *et al.*, *ChemRxiv.*, 2025, preprint, chemrxiv-2025-3f6br, DOI: 10.26434/chemrxiv-2025-3f6br.
5 Y. Zhang, C. He, K. de La Harpe, P. M. Goodwin, J. T. Petty and B. Kohler, *J. Chem. Phys.*, 2021, **155**, 094305.
6 R. R. Ramazanov, R. T. Nasibullin, D. Sundholm, T. Kurtén and R. R. Valiev, *J. Phys. Chem. Lett.*, 2024, **15**, 10710–10717.
7 H.-C. Hsu, M.-C. Ho, K.-H. Wang, Y.-F. Hsu and C.-W. Chang, *New J. Chem.*, 2015, **39**, 2140–2145.
8 Y. Teng, X. Yang, L. Han and E. Wang, *Chem. – Eur. J.*, 2014, **20**, 1111–1115.
9 D. Schultz, K. Gardner, S. S. R. Oemrawsingh, N. Markešević, K. Olsson, M. Debord, D. Bouwmeester and E. Gwinn, *Adv. Mater.*, 2013, **25**, 2797–2803.
10 J. T. Petty, J. Zheng, N. V. Hud and R. M. Dickson, *J. Am. Chem. Soc.*, 2004, **126**, 5207–5212.
11 C. J. Setzler, C. A. Arrington, D. Lewis and J. T. Petty, *J. Phys. Chem. B*, 2023, **127**, 10851–10860.
12 D. Lewis, C. Setzler, P. M. Goodwin, K. Thomas, M. Branham, C. A. Arrington and J. T. Petty, *J. Phys. Chem. C*, 2023, **127**, 10574–10584.
13 S. M. Swasey, F. Rosu, S. M. Copp, V. Gabelica and E. G. Gwinn, *J. Phys. Chem. Lett.*, 2018, **9**, 6605–6610.
14 A. Ono, S. Cao, H. Togashi, M. Tashiro, T. Fujimoto, T. Machinami, S. Oda, Y. Miyake, I. Okamoto and Y. Tanaka, *Chem. Commun.*, 2008, 4825–4827.
15 J. Müller, *Coord. Chem. Rev.*, 2019, **393**, 37–47.
16 C. López-Chamorro, A. Pérez-Romero, A. Domínguez-Martín, U. Javornik, O. Palacios, J. Plavec and M. A. Galindo, *Inorg. Chem.*, 2025, **64**, 14455–14465.
17 C. Cerretani, H. Kanazawa, T. Vosch and J. Kondo, *Angew. Chem., Int. Ed.*, 2019, **58**, 17153–17157.
18 G. Romolini, H. Kanazawa, C. B. Mollerup, M. B. Liisberg, S. W. Lind, Z. Huang, C. Cerretani, J. Kondo and T. Vosch, *Small Struct.*, 2025, **6**, 2500022.
19 D. J. E. Huard, A. Demissie, D. Kim, D. Lewis, R. M. Dickson, J. T. Petty and R. L. Lieberman, *J. Am. Chem. Soc.*, 2019, **141**, 11465–11470.

